University of Plymouth

PEARL **https://pearl.plymouth.ac.uk**

Faculty of Science and Engineering School of Engineering, Computing and Mathematics

2022-09-09

Wave interaction and energy absorption from arrays of complex-shaped point absorbers

Liu, Y

http://hdl.handle.net/10026.1/19832

10.1063/5.0107914
Physics of Fluids
American Institute of Physics

All content in PEARL is protected by copyright law. Author manuscripts are made available in accordance with publisher policies. Please cite only the published version using the details provided on the item record or document. In the absence of an open licence (e.g. Creative Commons), permissions for further reuse of content should be sought from the publisher or author.

Physics of Fluids

Wave interaction and energy absorption from arrays of complex-shaped point absorbers

Cite as: Phys. Fluids **34**, 097107 (2022); https://doi.org/10.1063/5.0107914
Submitted: 07 July 2022 • Accepted: 12 August 2022 • Accepted Manuscript Online: 13 August 2022 • Published Online: 09 September 2022

Yingyi Liu (刘盈溢), Siming Zheng (郑思明), Hui Liang (梁辉), et al.

View Online Export Citation CrossMark

ARTICLES YOU MAY BE INTERESTED IN

A heaving system with two separated oscillating water column units for wave energy conversion
Physics of Fluids **34**, 047103 (2022); https://doi.org/10.1063/5.0086581

Hydrodynamics of a floating liquid-tank barge adjacent to fixed structure in beam waves
Physics of Fluids **34**, 047114 (2022); https://doi.org/10.1063/5.0089127

Splitting dynamics of droplet impact on ridged superhydrophobic surfaces
Physics of Fluids **34**, 092104 (2022); https://doi.org/10.1063/5.0105634

Physics of Plasmas Physics of Fluids
Special Topic: Turbulence in Plasmas and Fluids
Submit Today!

AIP Publishing

© 2022 Author(s).

Physics of Fluids ARTICLE scitation.org/journal/phf

Wave interaction and energy absorption from arrays of complex-shaped point absorbers

Cite as: Phys. Fluids **34**, 097107 (2022); doi: 10.1063/5.0107914
Submitted: 7 July 2022 · Accepted: 12 August 2022 ·
Published Online: 9 September 2022

View Online Export Citation CrossMark

Yingyi Liu (刘盈溢),[1,a] Siming Zheng (郑思明),[2,b] Hui Liang (梁辉),[3] and Peiwen Cong (丛培文)[4]

AFFILIATIONS

[1]Research Institute for Applied Mechanics, Kyushu University, Fukuoka 8168580, Japan
[2]School of Engineering, Computing and Mathematics, University of Plymouth, Drake Circus, Plymouth PL4 8AA, United Kingdom
[3]Technology Centre for Offshore and Marine, Singapore (TCOMS), Singapore 118411, Singapore
[4]State Key Laboratory of Coastal and Offshore Engineering, Dalian University of Technology, Dalian 116024, China

[a)]**Email:** liuyingyi@riam.kyushu-u.ac.jp
[b)]**Author to whom correspondence should be addressed:** siming.zheng@plymouth.ac.uk

ABSTRACT

Water wave interactions with arrays of wave energy converters are numerically investigated based on the interaction theory. The converter is a heaving point absorber that can harness the ocean wave energy through up-and-down movements. A semi-analytical hybrid method is developed that combines the boundary element method and the interaction theory. The developed numerical method is verified against theoretical solutions for arrays of truncated vertical circular cylinders. Three different array layouts are studied in detail. It is found that trapped waves exist at critical wave numbers just below the cutoff values, and the peak load on the middle device increases with the number of devices in head waves. With the increase in the complexity of the array layout, significant wave force enhancement is observed, leading to a broader range of magnitude and stronger variations over the frequency band in beam waves. Moreover, variations of the q-factor show that there are some remarkable "bright spot" regions, indicating that the wave energy absorption there is locally optimized against wave conditions. By arranging the layout in a more randomized way, the optimal conditions for maximized power output can be hard to achieve, but the maximum power output can increase to a higher level.

© 2022 Author(s). All article content, except where otherwise noted, is licensed under a Creative Commons Attribution (CC BY) license (http://creativecommons.org/licenses/by/4.0/). https://doi.org/10.1063/5.0107914

I. INTRODUCTION

Wave power is one of the abundant and promising natural energy resources in vast oceans that has attracted intensive attention since 40 years ago (Isaacs and Schmitt, 1980). Up to the most recent decade, research on various aspects of utilizing the ocean wave power has been carried out, including but not limited to resource assessment (Iglesias and Carballo, 2010; Barbariol *et al.*, 2013), device modeling (Guo *et al.*, 2017; Ogden *et al.*, 2021; Cheng *et al.*, 2019; Wang *et al.*, 2022), control strategy (Faedo *et al.*, 2021; Parrinello *et al.*, 2020), and mooring design (Xu *et al.*, 2020; Paduano *et al.*, 2020). Furthermore, nowadays commercialization in the form of large-scale wave energy arrays is also under discussion (Gomes *et al.*, 2020; Pennock *et al.*, 2022).

A typical wave energy array is usually composed of a sequence of individual wave energy converters arranged periodically in an open sea region. One of the key scientific questions is how the existence of each device influences the performance of the others, which in essence comes to the hydrodynamic interaction problem between multiple floating bodies. A benchmark study in this field was undertaken by Maniar and Newman (1997) who investigated wave interactions with a uniform line array of identical, equally spaced, bottom-mounted vertical circular cylinders. The ratio of spacing to wavelength was identified as an important factor for the wave force variation. It was found that large wave excitation forces can be produced at certain frequencies in correspondence to the trapped modes present in an infinite periodic linear array, and the force on the cylinders near the center of the array increases with the number of cylinders. Inspired by the work of Maniar and Newman (1997), Evans and Porter (1997; 1999) studied the "near trapping" phenomenon in the scenario of a circular array of identical, equally spaced, bottom-mounted vertical circular cylinders by using the theory developed by Linton and Evans (1990). It was shown that large peaks in the forces on circular arrays of four, five, and six cylinders develop with the reduction of the gap between the cylinders. Subsequently, wave interactions with arrays of cylinders

were further extended to wave interaction theory in linear waves (Flavià *et al.*, 2018; Flavià and Meylan, 2019), second-order weakly nonlinear regular waves (Ohl *et al.*, 2001; Malenica *et al.*, 1999), fully nonlinear waves (Wang and Wu, 2010; Bai *et al.*, 2014), and transient waves (Wang and Wu, 2007; Meylan and Eatock Taylor, 2009). A systematic but relatively ancient review was presented in McIver (2002).

From the viewpoint of energy absorption, a scientific metric known as the interaction factor or the "q-factor" has been proposed in the literature to evaluate the performance of an entire wave farm (Babarit, 2013; Wolgamot *et al.*, 2012). The hydrodynamic interaction between individual devices can indeed lead to strong variations of such a metric compared to the scenario, assuming that no interaction exists. In this aspect, scholars have made substantial effort. Garnaud and Mei (2009) examined theoretically the power extraction by a compact periodic array of small buoys that do not resonate but possess many degrees of freedom in typical sea conditions. Child and Venugopal (2010) theoretically modeled the hydrodynamics of a wave energy device array in terms of the q-factor and looked for the optimal configuration using the Genetic Algorithm. Konispoliatis and Mavrakos (2016) analyzed an array of oscillating water column devices floating independently in finite depth waters and exposed to the action of regular surface waves based on the multiple scattering approach. Göteman (2017) presented an analytical model for point-absorbing wave energy converters connected to floats of cylinder or cylinder with a moonpool and assessed the impact of different layouts on wave energy parks with point absorbers. Zheng *et al.* (2018) developed a semi-analytical model for the wave interactions in a hybrid wave farm consisting of oscillating water columns and point absorbers. Zhong and Yeung (2019) studied the surface-wave interactions among an array of wave-energy converters in which each device is modeled as a truncated cylinder and investigated the interaction effects on power absorption from the array.

It is seen, however, that the aforementioned research in regard to the wave interactions with an array of floating bodies, each of the individual bodies in the array was generally assumed to be of regular shapes, e.g., a cylindrical or spherical geometry. In the literature, there have been quite rare research considering a non-regular geometry for an array. This is typically due to the known limitation of theoretical methods that are usually restricted to regular-shaped boundaries. In the present work, the foregoing drawback is overcome by developing a hybrid method that incorporates the wave interaction theory proposed in Kagemoto and Yue (1986) with the boundary element method as described in Liu (2019). With the facility of the hybrid method, large-scale computations can be conducted and the complexity of the wave interactions with arrays of bodies having non-regular geometries can be explored in detail. Furthermore, it is interesting to know how the interaction develops when the layout arrangement evolves from a simpler to a more complex one and the resultant effect on the wave energy absorption.

The remainder of this paper is organized as follows. Section II presents the mathematical theory and the modeling methodology for solving wave diffraction and radiation by multiple floating bodies. Section III verifies the resultant computation method via a comparison with benchmark results determined by theoretical methods. In Sec. IV, the present method is applied to three different array layouts that consist of identical CorPower-like WEC devices having a non-regular geometry. The layout effect on the wave loading of individual devices in the array and the possibility to achieve synthetic maximization of the power performance are analyzed in detail against various sea conditions. Finally, conclusions are drawn in Sec. V.

II. THEORY AND MODELING

In this section, the mathematical theory and the modeling methodology are presented for the wave interactions with multiple floating bodies, under the assumption that the fluid is incompressible and inviscid, and the flow is irrotational. Detailed formulations are given in the subsections below.

A. Ambient incident plane wave

Let us consider a train of regular incident waves that propagates to the positive x-direction with a small amplitude A, a heading angle β measured from the positive x-axis, and a wave number k, in water of a finite depth h. The ambient wave potential incident to body j can be written as

$$\phi_j^A(x_j, y_j, z_j) = -\frac{\mathrm{i}gA}{\omega}\frac{\cosh k(z_j+h)}{\cosh kh}\mathrm{e}^{\mathrm{i}k\left[(x_j+\bar{x}_j)\cos\beta+(y_j+\bar{y}_j)\sin\beta\right]}, \quad (1)$$

where $(\bar{x}_j, \bar{y}_j, 0)$ refers to the origin of the local coordinate system of body j in terms of the global Cartesian coordinates and (x_j, y_j, z_j) refers to an arbitrary spatial point in terms of the local Cartesian coordinates. By converting the local Cartesian coordinates to the polar coordinates (r_j, θ_j, z_j), Eq. (1) can be expanded as a summation of partial cylindrical waves incident to the body j,

$$\phi_j^A(r_j, \theta_j, z_j) = -\frac{\mathrm{i}gA}{\omega}\frac{\cosh k(z_j+h)}{\cosh kh}\mathrm{e}^{\mathrm{i}k(\bar{x}_j\cos\beta+\bar{y}_j\sin\beta)} \times \sum_{q=-\infty}^{\infty} J_q(kr_j)\mathrm{e}^{\mathrm{i}q(\pi/2+\theta_j-\beta)}, \quad (2)$$

where J_q denotes the Bessel function of the first kind of order q. For the sake of subsequent computations, Eq. (2) can be further written as the following compact form:

$$\phi_j^A(x_j, y_j, z_j) = \{a_j^I\}^T\{\psi_j^I\}, \quad (3)$$

in which the expansion coefficients are

$$\left\{a_j^I\right\}_{lq} = \begin{cases} -\mathrm{i}\dfrac{gA}{\omega}\mathrm{e}^{\mathrm{i}k\left(\bar{x}_j\cos\beta+\bar{y}_j\sin\beta\right)}\mathrm{e}^{\mathrm{i}q(\pi/2-\beta)}, & l=0, \\ 0, & l\geq 1, \end{cases} \quad (4)$$

while $\{\psi_j^I\}$ is a scalar vector of the basis function that is also named as the incident partial wave component (McNatt *et al.*, 2015; Flavià *et al.*, 2018)

$$\left\{\psi_j^I\right\}_{lq} = \begin{cases} \dfrac{\cosh k(z_j+h)}{\cosh kh}J_q(kr_j)\mathrm{e}^{\mathrm{i}q\theta_j}, & l=0, \\ \cos k_l(z_j+h)I_q(k_lr_j)\mathrm{e}^{\mathrm{i}q\theta_j}, & l\geq 1, \end{cases} \quad (5)$$

where l represents numbering of the eigen-expansion mode and I_q denotes the modified Bessel function of the first kind of order q.

© Author(s) 2022

B. Wave scattering amongst multiple floating bodies

In arrays of floating bodies, each individual body experiences not only the ambient incident plane wave but also the outgoing waves that are scattered from all the other neighboring bodies in the arrays. As sketched in Fig. 1, based on Graf's addition theorem (Abramowitz and Stegun, 1964), it is straightforward to obtain

$$H_m(kr_i)e^{im\theta_i} = \sum_{q=-\infty}^{\infty} H_{m+q}(kL_{ij})J_q(kr_j)e^{i[\alpha_{ij}(m+q)+q(\pi-\theta_j)]}, \quad (6)$$

$$K_m(k_nr_i)e^{im\theta_i} = \sum_{q=-\infty}^{\infty} K_{m+q}(k_nL_{ij})I_q(k_nr_j)e^{i[\alpha_{ij}(m+q)+q(\pi-\theta_j)]}, \quad (7)$$

where $H_m = J_m + iY_m$ denotes the Hankel function of the first kind of order m and K_m denotes the modified Bessel function of the second kind of order m. L_{ij} and α_{ij} represent the center-to-center distance and the angle, respectively, of $\overrightarrow{O_iO_j}$. The scattered waves from body i can then be expressed as incident waves to body j with the aid of a T-transfer matrix,

$$\phi_i^S(r_i, \theta_i, z_i) = \{A_i^S\}^T[T_{ij}]\{\psi_j^I\}, \quad (8)$$

where $\{A_i^S\}$ is a scalar vector of the scattering coefficients, the superscript "T" denotes the operation of transpose, and the T-transfer matrix reads

$$[T_{ij}]_{nn}^{mq} = \begin{cases} H_{m-q}(kL_{ij})e^{i\alpha_{ij}(m-q)}, & n = 0, \\ K_{m-q}(k_nL_{ij})e^{i\alpha_{ij}(m-q)}(-1)^q, & n \geq 1. \end{cases} \quad (9)$$

Note that Eq. (9) holds true for any integer m and any non-negative integer n, when $r_j \leq L_{ij}$.

On the basis of Eq. (8), the total wave potential that incidents to body j can be expressed as a summation of the ambient incident plane wave and all scattered waves from the other bodies

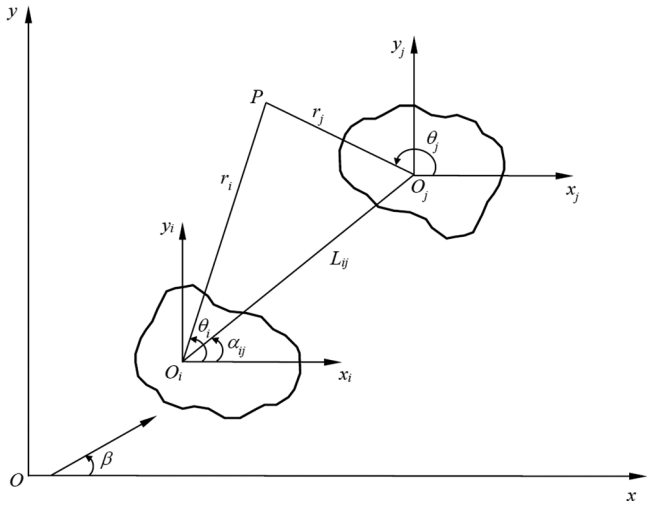

FIG. 1. Schematic of the local and global coordinate systems.

$$\phi_j^I(r_j, \theta_j, z_j) = \phi_j^A(r_j, \theta_j, z_j) + \sum_{\substack{i=1 \\ i\neq j}}^{N_B} \{A_i^S\}^T[T_{ij}]\{\psi_j^I\}$$
$$= \left(\{a_j^I\}^T + \sum_{\substack{i=1 \\ i\neq j}}^{N_B} \{A_i^S\}^T[T_{ij}]\right) \cdot \{\psi_j^I\}$$
$$(j = 1, 2, \ldots, N_B), \quad (10)$$

where N_B stands for the number of bodies in the arrays.

Using a so-called diffraction transfer matrix $[D_j]$ as the form that is defined in Liu *et al.* (2021) based on the hybrid dipole-source formulation, the scattered wave from body j and all the incident waves to the same body can be connected based on the following relation:

$$\{A_j^S\} = [D_j] \cdot (\{a_j^I\} + \sum_{\substack{i=1 \\ i\neq j}}^{N_B} [T_{ij}]^T\{A_i^S\}) \quad (j = 1, 2, \ldots, N_B) \quad (11)$$

from which the scattering coefficients can be solved numerically.

Wave excitation forces can, therefore, be calculated via pressure integration over each body and using matrix operations:

$$F_{j,p}^E = \left\{\eta_j^E\right\}^T\left\{G_{j,p}^E\right\}, \quad (12)$$

where $F_{j,p}^E$ is interpreted as the excitation force in the pth degree of freedom of body j. $G_{j,p}^E$ is the force transfer matrix with the following form:

$$\left\{G_{j,p}^E\right\} = i\omega\rho\int\int_{S_B^j}\left(\left\{\psi_j^I\right\} + [D_j]^T\left\{\psi_j^S\right\}\right)n_{j,p}dS, \quad (13)$$

where $n_{j,p}$ is the pth component of the normal vector on the immersed body surface, S_B^j is the immersed body surface, and ρ is the water density. The overall expansion coefficients of the total waves that incident to body j due to scattering of the ambient incident waves yield

$$\left\{\eta_j^E\right\}^T = \left\{a_j^I\right\}^T + \sum_{\substack{i=1 \\ i\neq j}}^{N_B} \{A_i^S\}^T[T_{ij}]. \quad (14)$$

The total wave $\{\eta_j^E\}$ consists of the ambient incident wave and all the scattered waves from neighboring bodies.

Following a similar approach, wave radiation forces acting on body j can be evaluated as

$$F_{j,t}^{R,i,p} = \begin{cases} \left\{\eta_j^{R,i,p}\right\}^T\left\{G_{j,t}^E\right\}, & i \neq j, \\ i\rho(a_{i,p} + \omega b_{i,p}) + \left\{\eta_j^{R,i,p}\right\}^T\left\{G_{j,t}^E\right\}, & i = j, \end{cases} \quad (15)$$

where $a_{j,p}$ and $b_{j,p}$ are, respectively, the added mass and the radiation damping of body j in the pth degree of freedom due to its own unitary motion in the same mode when the body is in isolation. Note that $F_{j,t}^{R,i,p}$ is interpreted as the radiation force of body j in the tth degree of freedom due to the motion of body i in pth degree of freedom. Correspondingly, the added mass and the radiation damping of a body can be obtained by decomposition of the complex radiation force

© Author(s) 2022

into real and imaginary parts. The overall expansion coefficient in association with the force transfer matrix reads

$$\left\{\eta_j^{R,i,p}\right\}^T = \left\{a_j^{R,i,p}\right\}^T + \sum_{\substack{s=1 \\ s\neq j}}^{N_B} \left\{A_s^{R,i,p}\right\}^T [T_{sj}], \tag{16}$$

where $\{a_j^{R,i,p}\}$ are the expansion coefficients of the radiated wave incident on body j, generated by the unitary motion of body i in its pth degree of freedom,

$$\left\{a_j^{R,i,p}\right\} = \begin{cases} 0, & i = j, \\ [T_{ij}]^T \cdot \{R_i^p\}, & i \neq j, \end{cases} \tag{17}$$

where $\{R_i^p\}$ is termed as radiation characteristics as defined in Liu *et al.* (2021). $\{A_s^{R,i,p}\}$ is the total waves that incident to body j due to the scattering of radiated waves, which can be solved from the following linear algebraic system:

$$\{A_j^{R,i,p}\} = [D_j] \cdot (\{a_j^{R,i,p}\} + \sum_{\substack{s=1 \\ s\neq j}}^{N_B} [T_{sj}]^T \{A_s^{R,i,p}\}) \quad (j = 1, 2, \ldots, N_B). \tag{18}$$

C. Wave power and interaction factor

It is common to use the so-called interaction factor to evaluate the performance of arrays of wave energy converters. The interaction factor q is defined as a function of the wave number k and the incident wave angle β (Child and Venugopal, 2010)

$$q(k,\beta) = \frac{\sum_{j=1}^{N_B} P_j(k,\beta)}{N_B \times P_0(k,\beta)}, \tag{19}$$

where P_0 represents the wave power extracted by an isolated converter and P_j represents the wave power extracted by the jth device in the arrays. Physically, Eq. (19) indicates that if $q < 1$, the average extracted power per converter in the array is less than the power extracted by an isolated converter (Babarit, 2013). This means that wave interactions have a destructive effect on the power absorption of the wave farm. In contrast, if $q > 1$, the park effect is constructive. Evans (1979) and Falnes (1980) independently derived the maximum absorbed power of an entire array

$$\left(\sum_{j=1}^{N_B} P_j(k,\beta)\right)_{\max} = \frac{1}{8}\{F^E\}^* [B_{\text{rad}}]^{-1} \{F^E\}, \tag{20}$$

where $\{F^E\}$ is a scalar vector of complex amplitudes of the wave excitation forces; $[B_{\text{rad}}]$ represents the radiation damping matrix; and the asterisk $*$ denotes complex conjugate transpose. For wave energy converters having a vertical axis of symmetry, it is possible to derive an alternative relationship to calculate the interaction factor (Fitzgerald and Thomas, 2007)

$$q(k,\beta) = \frac{k}{N_B} \frac{\left(\sum_{j=1}^{N_B} P_j(k,\beta)\right)_{\max}}{P_W}, \tag{21}$$

where P_W is the time-averaged incident wave power per unit crest-width

$$P_W = \frac{\rho g A^2 \omega}{4k}\left(1 + \frac{2kh}{\sinh 2kh}\right). \tag{22}$$

Equation (22) is a derived form from Eq. (4.130) in Falnes and Kurniawan (2020).

III. VERIFICATION WITH THEORETICAL RESULTS

Numerical verifications are conducted by comparing with benchmark results calculated by other existing methods. We hereby select theoretical methods as the counterpart because of their proven high accuracy. In Secs. III A and III B, verifications on two cylindrical buoys and four cylindrical buoys are given, in order to demonstrate the validity of the present methodology in the respective computations for a linear array and a double array.

A. Two cylindrical buoys in a line array

At first, two cylindrical buoys are considered. The geometry of each buoy is a truncated vertical cylinder of radius $r = a$, draught $d = a/2$, being placed in water of depth $h = 10a$. Two cases are analyzed, having spacings between the axes of the cylinders of $s = 3a$ and $s = 5a$ (see Fig. 2), respectively. Each cylinder is discretized using 472 quadrilateral or triangular panels on the immersed hull surface and 232 panels on the cross-sectional waterplane area. This problem has been analyzed by Siddorn and Eatock Taylor (2008) using a theoretical method.

Figures 3 and 4 exhibit a comparison between the results produced from the present method and a theoretical method documented in Zheng *et al.* (2018). The results of Siddorn and Eatock Taylor (2008) are not included here due to the missing out of a factor of π. Modulus of the wave excitation forces $|F_x|$ and $|F_z|$ are nondimensionalized by $A\rho g\pi a^2$, where A is the amplitude of the incident wave. The present results in general have a good agreement in comparison with the theoretical results. In addition, one more interesting thing that can be observed is that a larger spacing $s = 5a$ tends to yield more variations than a smaller spacing $s = 3a$.

B. Four cylindrical buoys in a double array

A small array consisting of four cylindrical buoys is further considered. The geometry of each buoy is a truncated vertical cylinder of radius $r = a$, draught $d = 2a$, being placed in water of depth $h = 4a$. The foursquare layout of the array separates neighboring cylinders by a distance of $s = 4a$ for an incident wave heading angle of $\beta = \pi/4$ (see Fig. 5). Each cylinder is discretized using 1192 quadrilateral or triangular panels on the immersed hull surface and 232 panels on the cross-sectional waterplane area. This problem has been analyzed by

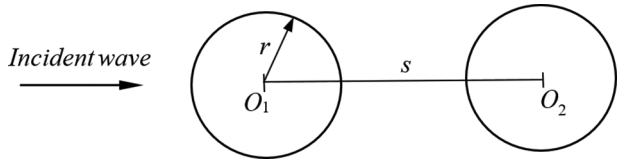

FIG. 2. Layout of the two cylindrical buoys.

© Author(s) 2022

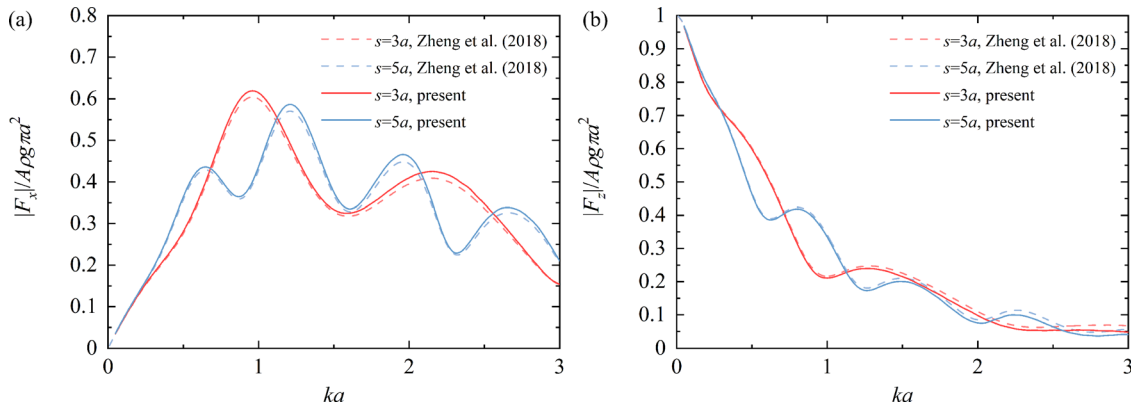

FIG. 3. Excitation forces on the weather-side cylinder: (a) horizontal force F_x and (b) vertical force F_z.

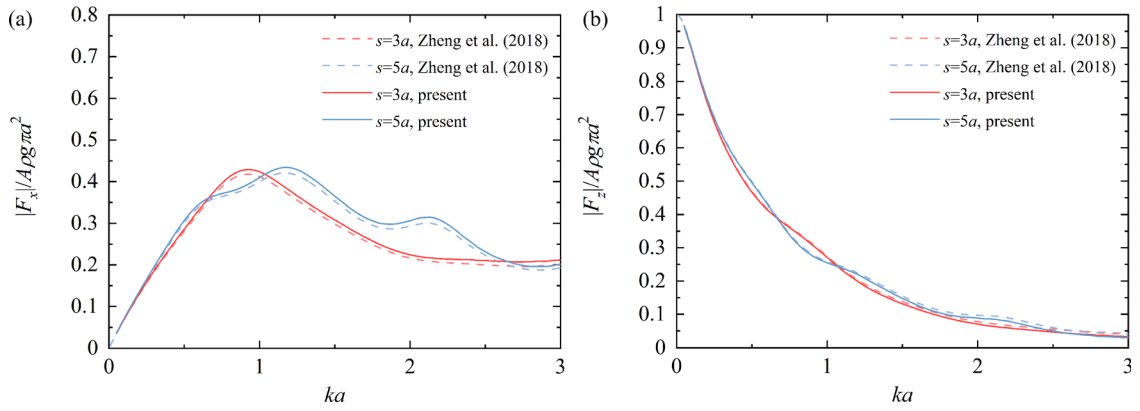

FIG. 4. Excitation forces on the lee-side cylinder: (a) horizontal force F_x and (b) vertical force F_z.

Siddorn and Eatock Taylor (2008) using the same theoretical method as for the two-cylinder case.

Figures 6–8 exhibit a comparison between the present results and those of Siddorn and Eatock Taylor (2008) and Zheng *et al.* (2018). It is noted that results of Siddorn and Eatock Taylor (2008) are not included in Fig. 6(b) since a factor of 1.4 seems to have been missed out in the horizontal wave excitation force $|F_x|$. In addition, Siddorn and Eatock Taylor (2008) did not present the usual added mass and radiation damping. However, their definition of the radiation impedance $Z_{i,j}$ follows the relationship of $Z = b_{i,j} + i\omega a_{i,j}$, where $a_{i,j}$ and $b_{i,j}$, respectively, refer to the added mass and radiation damping as defined in Eq. (15) of this paper. For the above reason, in Figs. 7 and 8, the theoretical results of Zheng *et al.* (2018) are, thereby, used for comparison of the hydrodynamic coefficients.

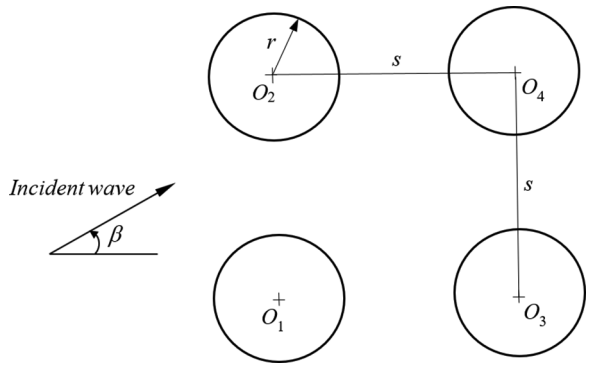

FIG. 5. Layout of the four cylindrical buoys.

IV. RESULTS AND DISCUSSION

The individual device adopted hereafter is a CorPower-like heaving point absorber (Faedo *et al.*, 2021) that harvests wave energy through up-and-down heave motions. The point absorber device is discretized using 765×4 panels on the immersed body surface and 46×4 panels on the waterplane cross-sectional area. The dimensions and the surface mesh of the device are given in Fig. 9. Note that the device consists of two circular cylindrical ends and a flipped frustum transition part. For brevity, we define the diameter of the upper cylindrical section as the characteristic diameter of the device, i.e., $D = D_1$.

© Author(s) 2022

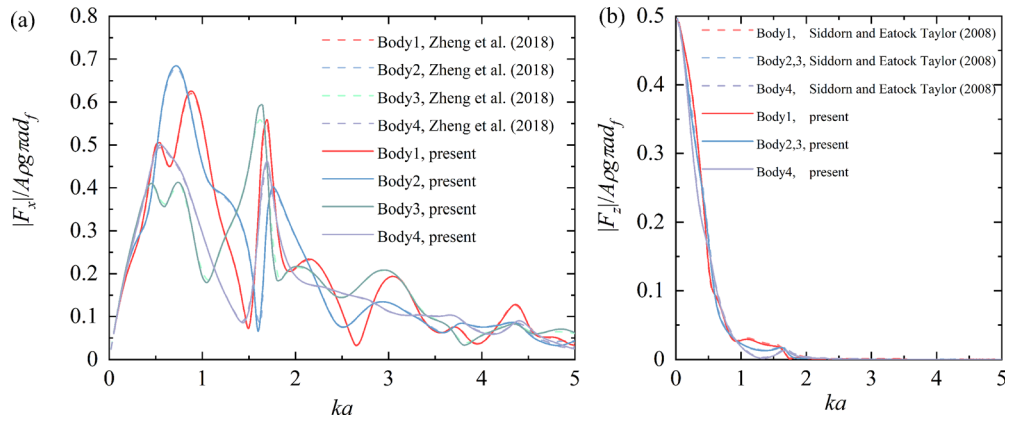

FIG. 6. Excitation forces, $\beta = \pi/4$: (a) vertical force F_x and (b) horizontal force F_z.

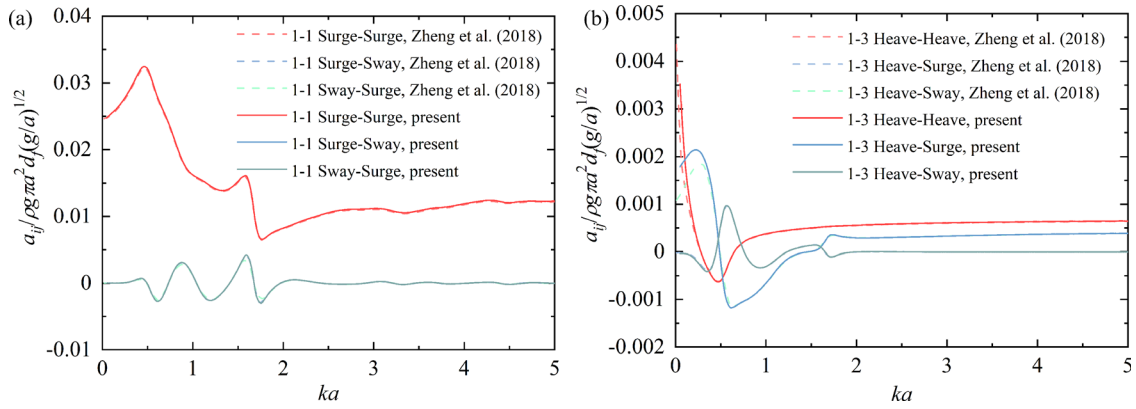

FIG. 7. Hydrodynamic coefficients of the rigid body modes of a single body: (a) added mass and (b) radiation damping.

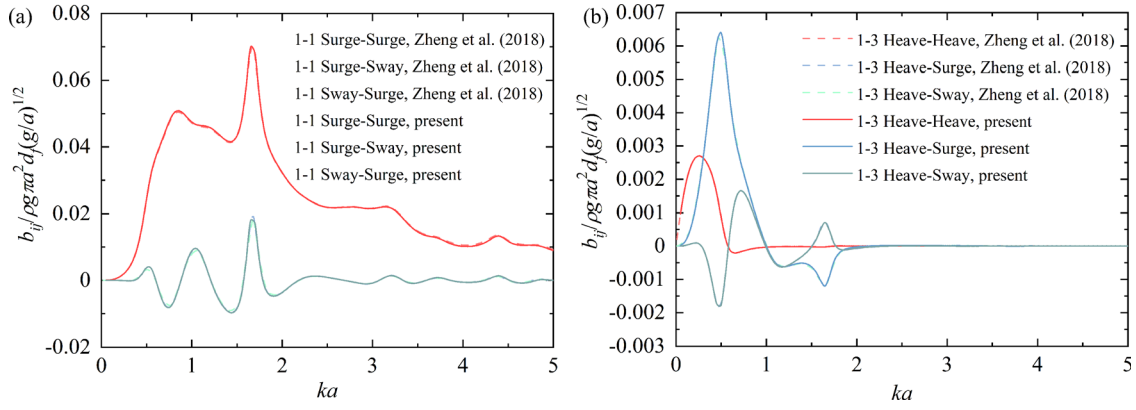

FIG. 8. Hydrodynamic coefficients of the rigid body modes between different bodies: (a) added mass and (b) radiation damping.

Wave interactions between arrays of point absorbers in a large wave farm involve complex physical mechanisms due to various layout possibilities. Although complicated, these mechanisms can be understood from some elemental arrangements.

A. A uniform line array of point absorbers

Wave interactions between a uniform line array of the CorPower-like device is considered first. The layout is given in Fig. 10. The spacing between two neighboring devices of the periodical array is

© Author(s) 2022

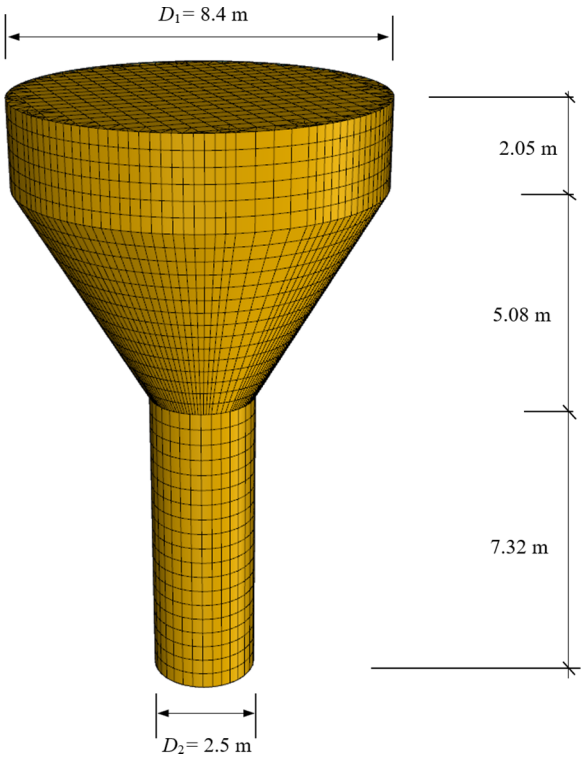

FIG. 9. Surface mesh and dimensions of the point absorber converter.

s, and d is half of the spacing, i.e., $d = s/2$. The N_B centers of the device cross-sectional areas are evenly located in a straight line.

Figure 11 exhibits the wave excitation forces on each body of a periodical array consisting of seven such devices in head waves, i.e., the case when incident waves propagate in the direction parallel to the array. The force magnitude is normalized by $\rho g V$, where V is the displaced volume of an individual device. The most distinctive feature of the longitudinal force F_x herein is that a sequence of narrow peaks occurs at the places where the wave interference parameter kd is slightly less than $n\pi/2$ $(n = 1, 2, \ldots)$. This finding is exactly similar to the case in Maniar and Newman (1997) regarding an array of bottom-mounted circular cylinders, known as Bragg resonance in many fluid physical phenomena (Li and Mei, 2007; Peng *et al.*, 2019; Zhao *et al.*, 2021; Gao *et al.*, 2021; Ning *et al.*, 2022). It is also found that the magnitude of the longitudinal force is smaller than that of a single device in isolation, except for the neighboring area within a narrow band enclosing the peaks. An analogical phenomenon can be found in the vertical force F_z, which does not present peaks, but rather troughs. Moreover, results of the lateral force F_y are not displayed here because they are all zeros in line with common knowledge.

In beam waves, i.e., the case when incident waves propagate in the direction perpendicular to the array, things become different. Figure 12 exhibits the results of a uniform line array of 9 such devices in beam waves. It is found that in the direction parallel to the array that is perpendicular to the wave incident direction, the longitudinal force F_x acting on each device is no longer zero, except the one in the middle of the line array. As the longitudinal force of an isolated single body is exactly zero under the same circumstance, the non-zero value of F_x in the array is believed to be caused by the interaction between

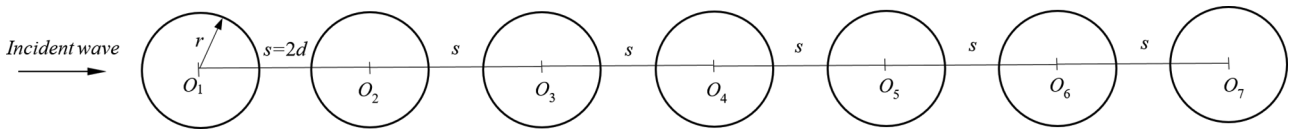

FIG. 10. Layout of a uniform line array of CorPower-like point absorbers.

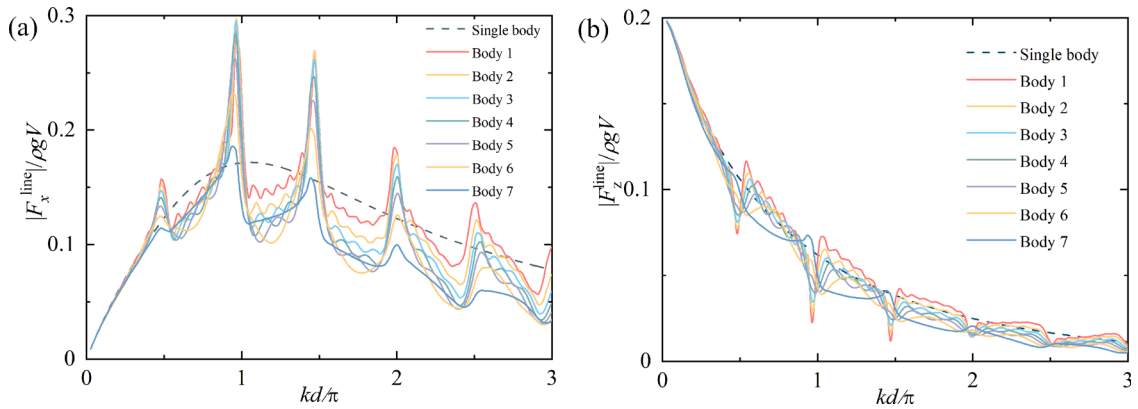

FIG. 11. Wave excitation forces of each device in a uniform line array of 7 bodies in head waves ($\beta = 0°$, $h = 50$ m, $s = 4D$): (a) longitudinal force F_x and (b) vertical force F_z.

© Author(s) 2022

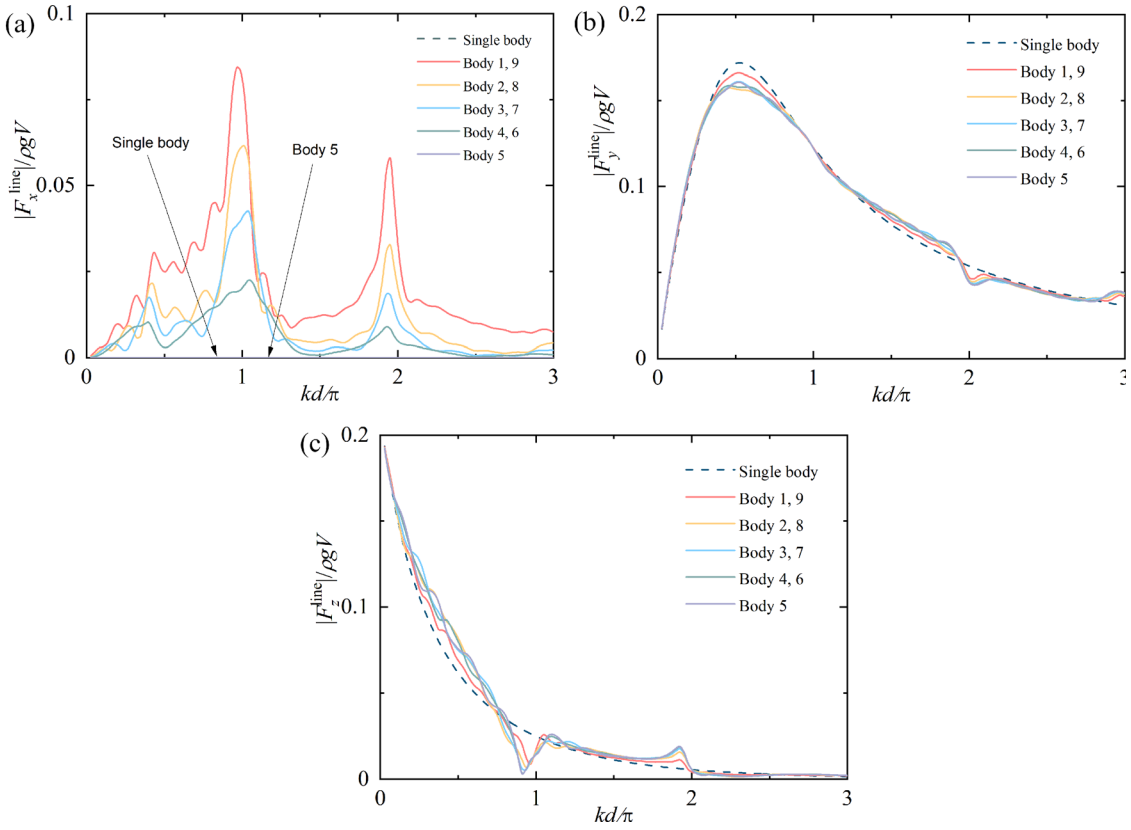

FIG. 12. Wave excitation forces of each device in a uniform line array of 9 bodies in beam waves ($\beta = 90°, h = 50\,\text{m}, s = 2D$): (a) longitudinal force F_x, (b) lateral force F_y, and (c) vertical force F_z.

individual devices of the array. Moreover, Fig. 12(a) shows that the longitudinal force decreases gradually from the two ends to the middle of the array. This should be attributed to the symmetrical property of the problem, which is also presented by Maniar and Newman (1997) in the case of a bottom-mounted cylinder array. The lateral and vertical forces on an individual device are in general similar to those of the others in the array as well as a single device in isolation, except for some small variations. These results elucidate that the wave interaction occurs primarily along the direction in parallel rather than perpendicular to the array.

Let us examine, thereby, the relationship between the longitudinal force against the number of devices in the uniform line array. In Fig. 13(a), it is found that in head waves, the peak load on the middle device (rigorously, the $[N_B/2]$th device) increases with the increase in

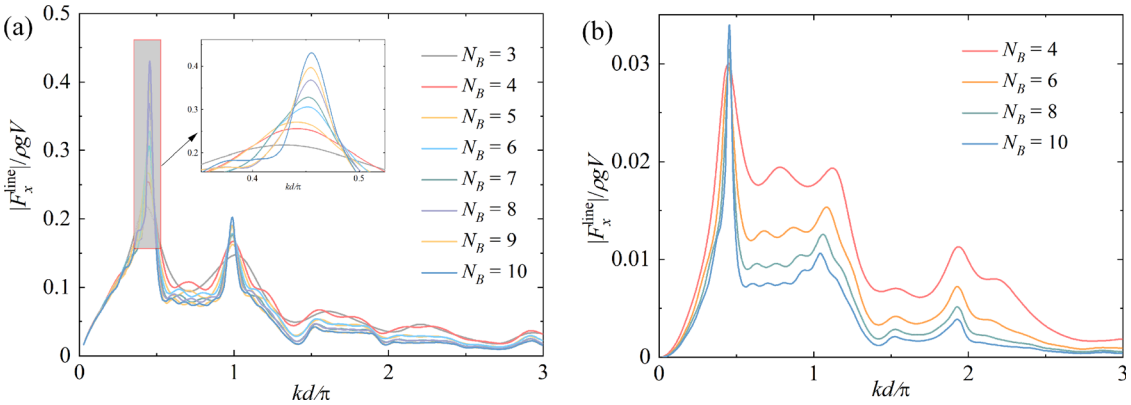

FIG. 13. Longitudinal force F_x acting on the $[N_B/2]$th device in the middle of the line array: (a) N_B bodies in head waves and (b) N_B bodies in beam waves.

© Author(s) 2022

the number of devices, whereas in beam waves, provided an odd number of devices, the longitudinal wave force F_x acting on the middle device turns to be zero and, hence, not displayed in Fig. 13(b). It can be found that in such an even array, the longitudinal wave load acting on the middle device (rigorously, the first device close to the middle) decreases with the increase in the number of devices, except in the neighborhood area around the peak.

Variations of the q-factor vs the device spacing s, the wave heading angle β, and the wave angular frequency ω for the uniform line array consisting of seven devices are shown in Fig. 14. The most distinctive result herein is that there are some remarkable "bright spot" regions, indicating that the wave energy absorption there is locally optimized against wave conditions. With regard to a uniform line array, it is found that the lower the wave frequency is, the larger the wave heading tends to be in association with the center of a spot region. In addition, the number or the density of the spot regions increases with the device spacing.

B. A double array of point absorbers in parallel arrangement

Wave interactions amongst a double array in parallel arrangement are investigated thereafter. The spacing between neighboring devices affiliated to either two rows or two columns remains the same as $s = 2d$. The corresponding layout is shown in Fig. 15.

Figure 16 depicts the results of a 2×7 array in a parallel arrangement in head waves. To achieve a better understanding, the force magnitude on each device in the double parallel array is normalized by that on the corresponding device at the same column of the uniform line array as given in Fig. 11, which is defined as "force enhancement ratio" herein. It is found that the force enhancement ratio of either the longitudinal or the vertical force generally ranges between 0.5 and 1.5, indicating no particular enhancement when there exists a parallel row side by side. In long wavelengths, e.g., in the regime approximately $kd/\pi < 0.3$, the ratio is close to unity, which means that the interaction between two rows of the array almost diminishes to zero. In addition, results on neighboring devices of the two rows are exactly the same since the problem is symmetrical in head waves.

In beam waves, however, apparent differences exist. Figure 17 depicts the force enhancement ratios of the wave forces acting on the front row (the row first attacked by the incident waves) of a 2×9 double parallel array over those of the corresponding uniform line array as given in Fig. 12, when waves come along the direction perpendicular to the array. Significant increases are found in the longitudinal and the vertical force magnitudes. The maximum peak value is approximately 6 times in the longitudinal load and 4.5 times in the vertical load, as compared to the loads acting on the devices of the uniform line array.

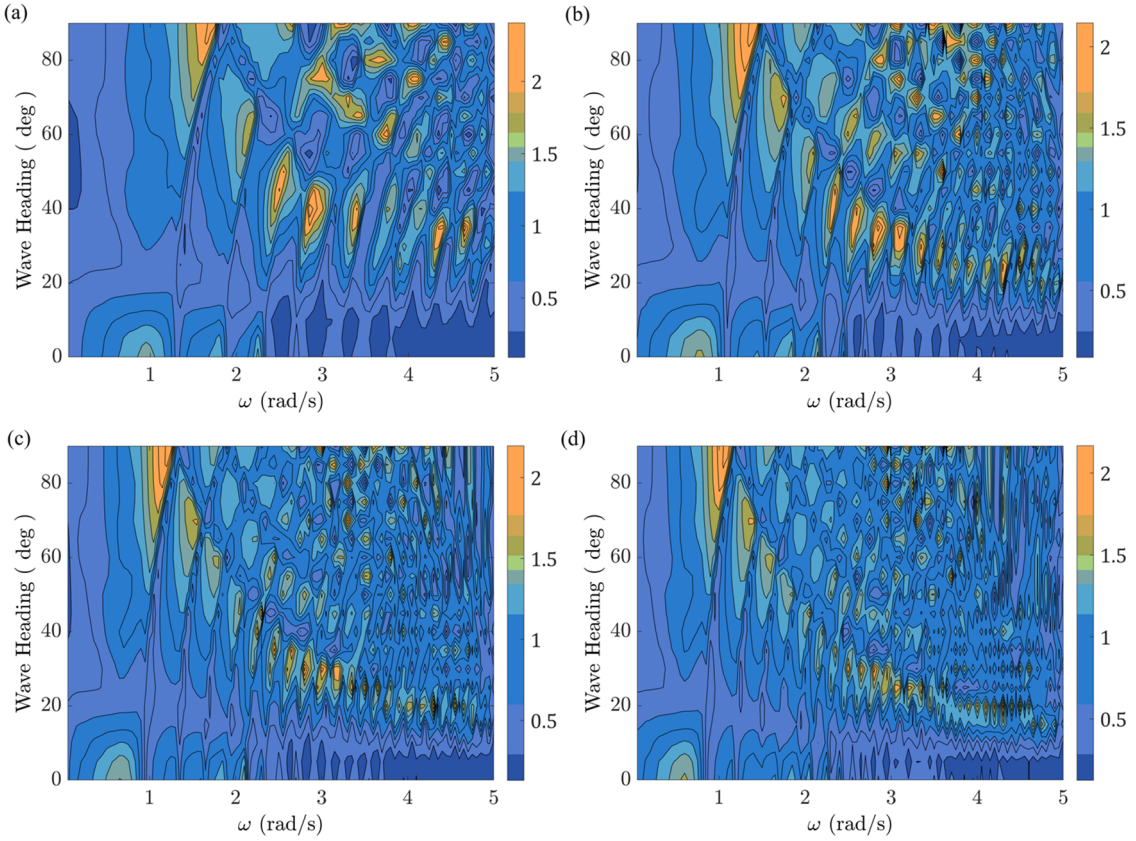

FIG. 14. q-factor variation of the uniform line array of CorPower-like point absorbers against the angular frequency ω, the wave heading β, and the device spacing s ($h = 100$ m): (a) $s = 2D$, (b) $s = 3D$, (c) $s = 4D$, and (d) $s = 5D$.

© Author(s) 2022

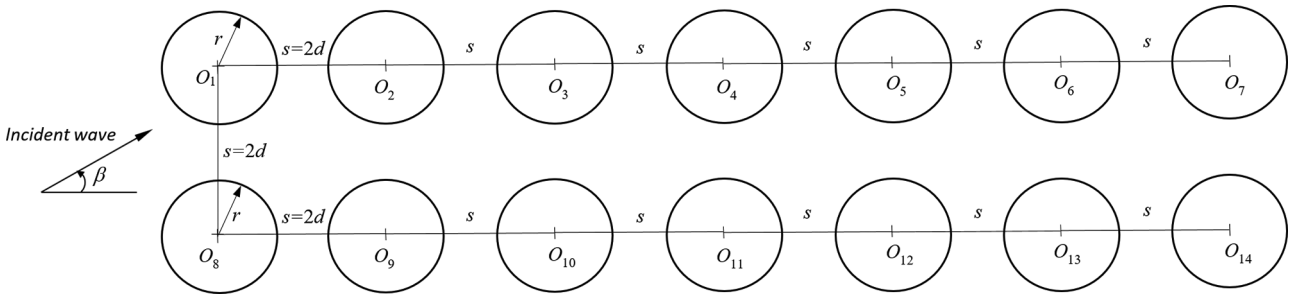

FIG. 15. Layout of a 2×7 double parallel array of CorPower-like point absorbers.

Again, the longitudinal force on the middle device of the front row (the 14th device) is zero, which is similar to that in the uniform line array as shown in Fig. 12.

Figure 18 presents the force enhancement ratios of the wave forces acting on the rear row (the row behind the front row) of the same double parallel array over those of the corresponding uniform line array, when waves incident from 90°. The maximum peak value of the force enhancement ratio increases to eight times in the longitudinal load and decreases to four times in the vertical load, as compared to the loads acting on the devices of the uniform line array. The maximum peak value of the lateral load remains unchanged at generally the same level. Again, the middle device of the rear row (the 5th device) endures no wave load, which is similar to that in the front row of the double parallel array.

The force enhancement ratios defined in Figs. 16–18 can describe the variation of wave forces of a double parallel array against the uniform line array. Unfortunately, such a definition involves a large degree of randomness due to the presence of wave interactions among both the two arrays. By changing the ratios to the ones on the basis of a single isolated device, the inherent nature of trapped modes can be found to exist as well for the double parallel array. Figure 19 shows that in head waves, remarkable peaks exist in both of the two arrays at critical wave numbers just below the cutoff value $kd = n\pi/2\,(n = 1, 2, \ldots)$, and the peak magnitude remains at a similar level. The difference lies in that the longitudinal force ratios of a double parallel array exhibit secondary peaks, which is in line with the ones discussed in (Zeng *et al.*, 2019) for arrays of bottom-mounted circular cylinders. The phenomenon of secondary peaks occurs especially at relatively higher wave numbers when $kd/\pi > 1.0$, indicating that the array interactions in short waves are more prone to be captured than in long waves.

Variations of the q-factor vs the device spacing s, the wave heading angle β, and the wave angular frequency ω for the 2×7 double parallel array are displayed in Fig. 20. It is found that the q-factor distributions of a double array are more randomized than those of a uniform line array, as compared to Fig. 14, indicating much stronger interactions among the devices since the scattered waves come from neighboring devices not only in a row but also in a column. In addition, the peaks at the locally optimized bright spot regions increase to much larger values than those of the uniform line array, which means a better synergy in the wave power absorption.

C. A double array of point absorbers in staggered arrangement

We further consider the wave interactions among a double array in a staggered arrangement. As shown in Fig. 21, along the direction in parallel to the array, the center of each device of the second row locates in the middle of the spacing between two neighboring devices of the first row. In other words, the second row is shifted to the right-hand side by a distance of $s/2$ from the original position in the double

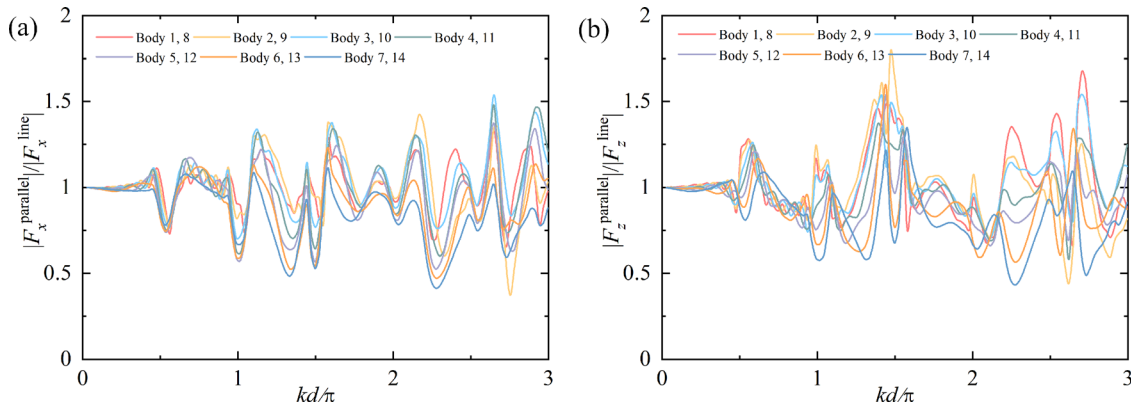

FIG. 16. Force enhancement ratios of the wave forces acting on a 2×7 double parallel array over those of the uniform line array in head waves ($\beta = 0°, h = 50$ m, $s = 4D$): (a) longitudinal force F_x and (b) vertical force F_z.

© Author(s) 2022

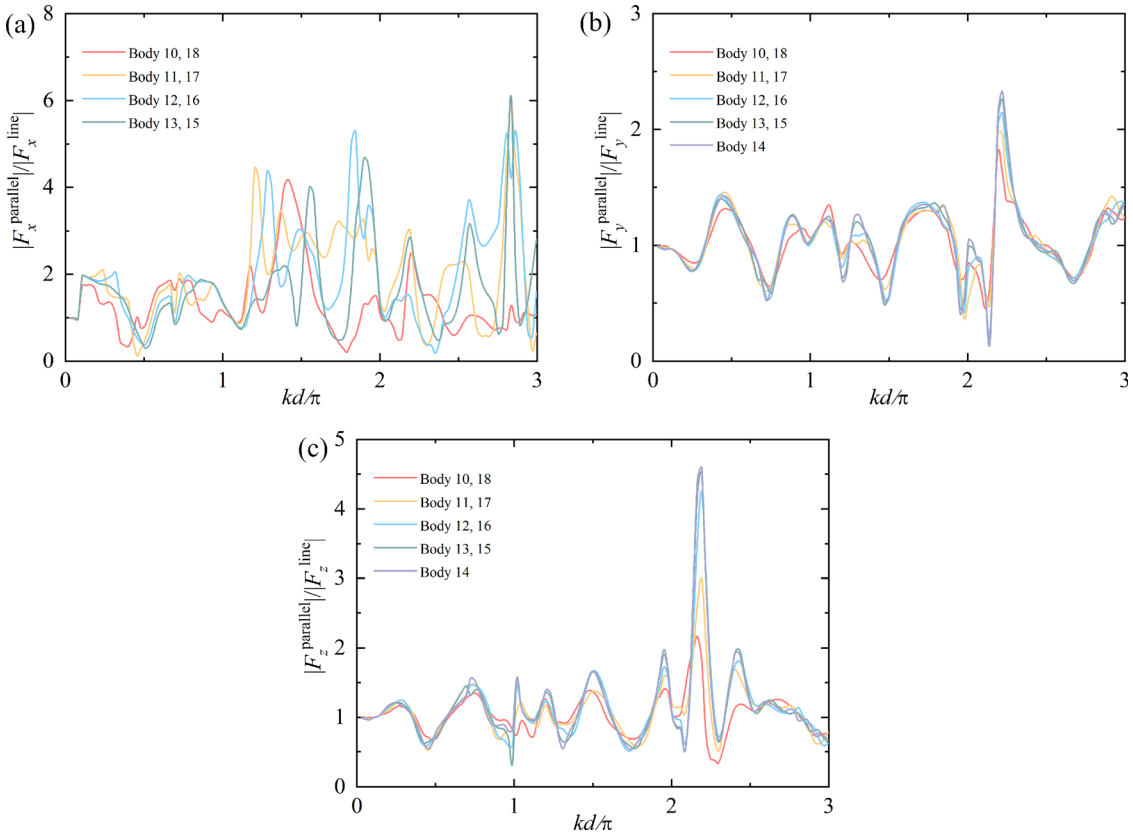

FIG. 17. Force enhancement ratios of the wave forces acting on the front row of a 2×9 double parallel array over those of the uniform line array in beam waves ($\beta = 90°, h = 50\,\text{m}, s = 2D$): (a) longitudinal force F_x, (b) lateral force F_y, and (c) vertical force F_z.

parallel array as given in Fig. 10. The distance between neighboring rows remains the same as $s = 2d$.

First, it is found that the staggered arrangement can lead to a particular phenomenon in beam waves. Figure 22 exhibits the force enhancement ratios of the lateral force F_y acting on a 2×9 double staggered array over that on a 2×9 double parallel array in beam waves. The force enhancement ratios are obtained for each body tagged with the same numbering in the two different arrangements. The results show that by arranging the double array in a staggered manner, the lateral force acting on the rear row can reach a small ratio close to zero in between a narrow bandwidth $kd/\pi \in [1.0, 1.5]$. The smallest ratio is 0.089 at the place $kd/\pi = 1.203$. An analogical phenomenon can be found for the front row at the place $kd/\pi = 2.487$, where the smallest value is 0.120. Figure 23 turns over the ratio to show more clearly. Large peaks in the inverse ratios are found concentrated on the narrow bandwidth $kd/\pi \in [1.0, 1.5]$ and the place around $kd/\pi = 2.5$.

Further studies show that this phenomenon exists in no relation to the overall number of devices in an array. Figure 24 depicts the force enhancement ratios of the lateral force F_y acting on a 2×5 double staggered array over that on a 2×5 double parallel array in beam waves. Although the number of devices in each row reduces to 5, similar phenomenon occurs in between the narrow bandwidth $kd/\pi \in [1.0, 1.5]$ and the place $kd/\pi = 2.487$. The smallest values are 0.011 and 0.094, respectively, close to zero. The above findings can be further confirmed by turning over the ratio as shown in Fig. 25.

These results elucidate that, when the device spacing ranges from 1 to 1.5 times or equals to approximately 2.5 times the wavelength (because of $kd/\pi = s/L$, where s is the device spacing and L is the wavelength), the wave forces acting on the bodies of the rear row of a double array can be significantly weakened by shifting the front row with a certain in-line distance from the parallel arrangement. Moreover, it is noted that in long wave regimes, e.g., $kd/\pi < 1.0$, the force enhancement ratios keep at the level of unity, indicating that in long waves, the staggered or parallel arrangement is not a factor for the interactions.

Figure 26 presents a comparison between the lateral force ratios of the three different arrays in beam waves. The force enhancement ratio of the lateral wave force herein is obtained by dividing its counterpart acting on a single isolated device. It is found that, by arranging an array layout into a more randomized manner, the lateral force ratio exhibits stronger variations over the entire frequency band. Specifically, the highest peak magnitude significantly increases with the change in a simpler layout to a more complex layout, and the lowest trough magnitude decreases to a smaller value approaching zero. As an example shown in Fig. 26, while the lateral force ratios of a

© Author(s) 2022

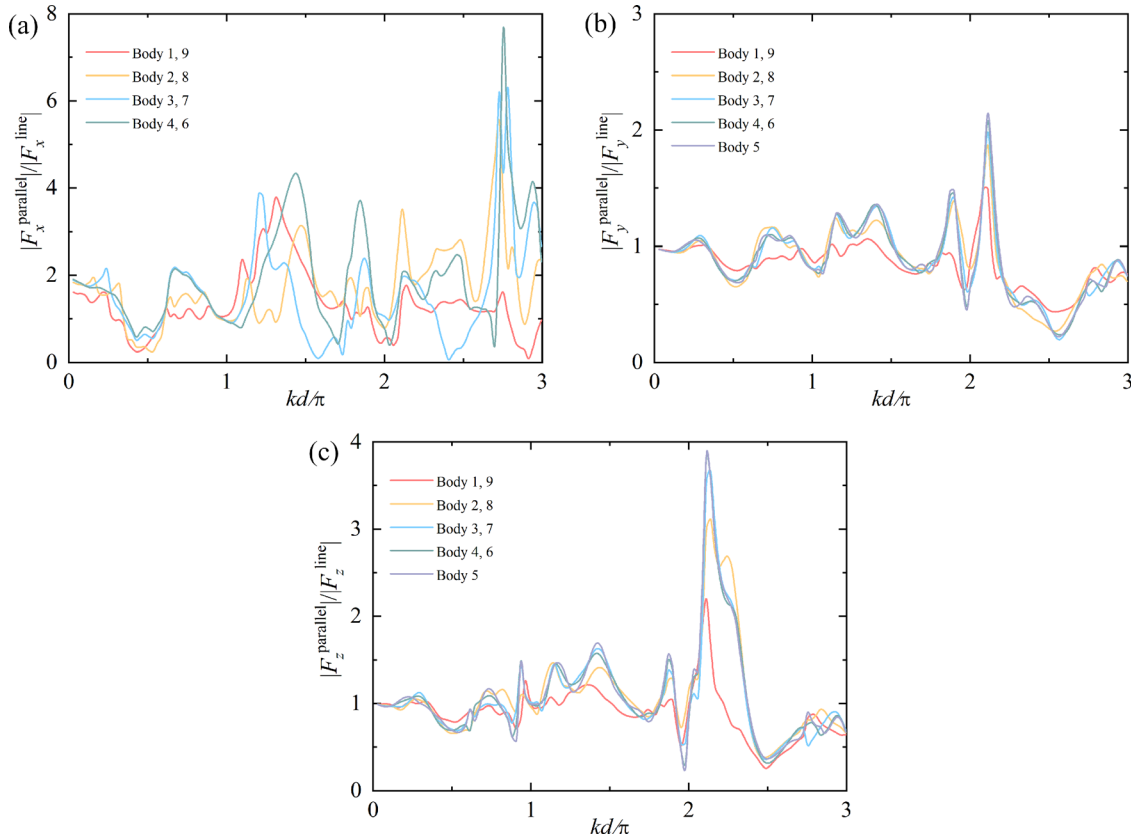

FIG. 18. Force enhancement ratios of the wave forces acting on the rear row of a 2×9 double parallel array over those of the uniform line array in beam waves ($\beta = 90°, h = 50\,\text{m}, s = 2D$): (a) longitudinal force F_x, (b) lateral force F_y, and (c) vertical force F_z.

uniform line array fall in between $[0.75, 1.25]$, the ones of a double parallel array range from $[0.25, 2.0]$, and the ones of a double staggered array range from $[0, 3.0]$.

Variations of the q-factor vs the device spacing s, the wave heading angle β, and the wave angular frequency ω for the 2×7 double staggered array are displayed in Fig. 27. It is found that in comparison with the ones of the double parallel array, as given in Fig. 20, the q-factor distributions of a double array in a staggered arrangement are even more randomized, indicating stronger interactions. The areas of the locally optimized bright spot regions are even smaller as compared to the parallel case. However, the peak values of the bright spot regions do increase. Moreover, with the expansion of the device spacing, the

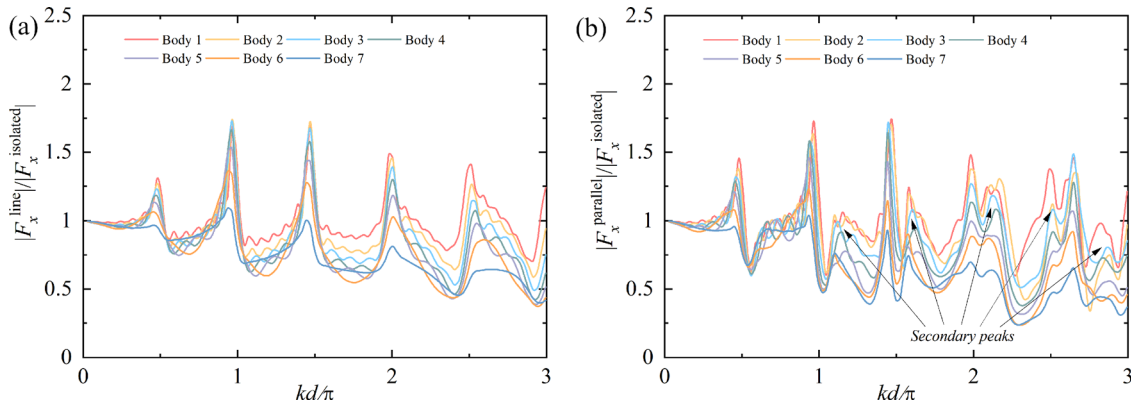

FIG. 19. Longitudinal force ratios of (a) a 1×7 uniform line array and (b) a 2×7 double parallel array over that of a single isolated device in head waves ($\beta = 0°, h = 50\,\text{m}, s = 4D$).

© Author(s) 2022

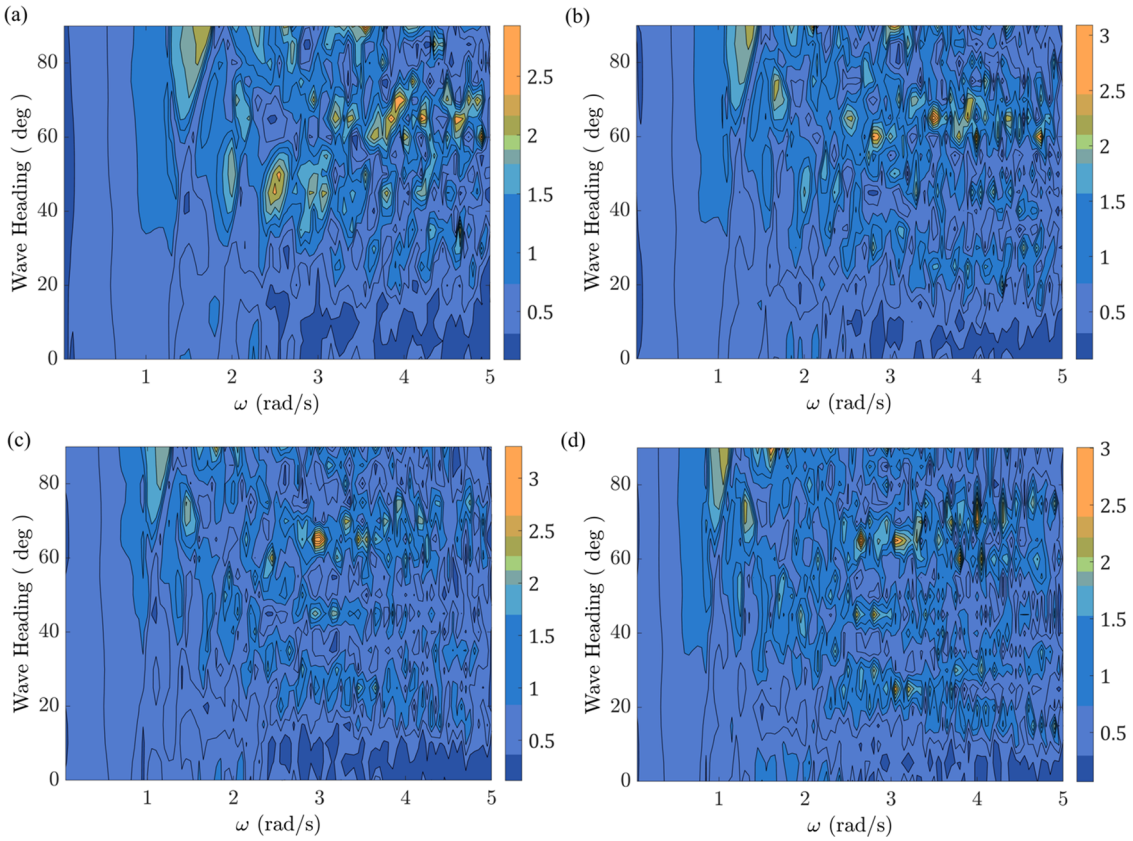

FIG. 20. q-factor variation of the double parallel array of CorPower-like point absorbers against the angular frequency ω, the wave heading β, and the device spacing s ($h = 100$ m): (a) $s = 2D$, (b) $s = 3D$, (c) $s = 4D$, and (d) $s = 5D$.

density of the optimized regions is also enhanced. All in all, the q-factor results in Figs. 14, 20, and 27 elucidate that by arranging the array layout in a more randomized way, though the optimal conditions for maximized power output can be hard to achieve, the maximum power output can increase to a higher level.

V. CONCLUSIONS

In this work, wave interaction and energy absorption from arrays of wave energy converters are investigated. The converter is a CorPower-like point absorber device that can harness the water wave energy from up-and-down heaving movements. Due to the reason that the device shape is more complex than a regular geometry, such as circular cylinders and spherical bodies, the usual analytical methods are no longer applicable. By developing a hybrid method that combines the boundary element method as described in Liu (2019) and the wave interaction theory as in Kagemoto and Yue (1986), the problem can be analyzed with ease. After verification of the method, wave energy arrays in three different layouts are studied in detail and the main conclusions are summarized below:

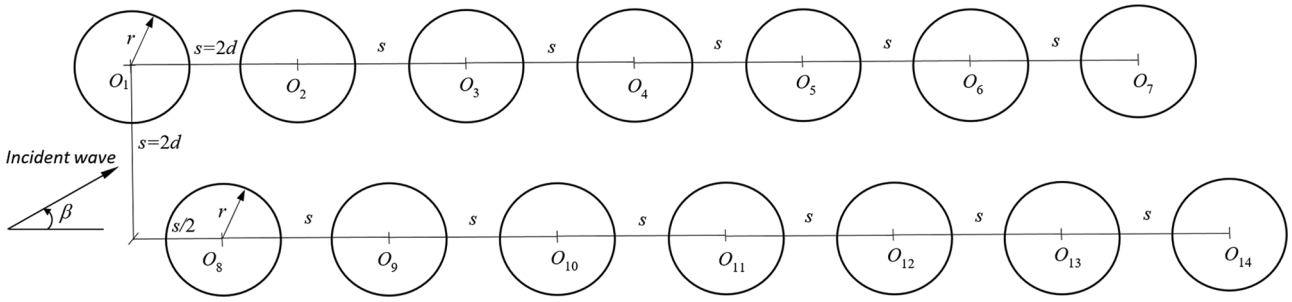

FIG. 21. Layout of a 2 × 7 double staggered array of CorPower-like point absorbers.

© Author(s) 2022

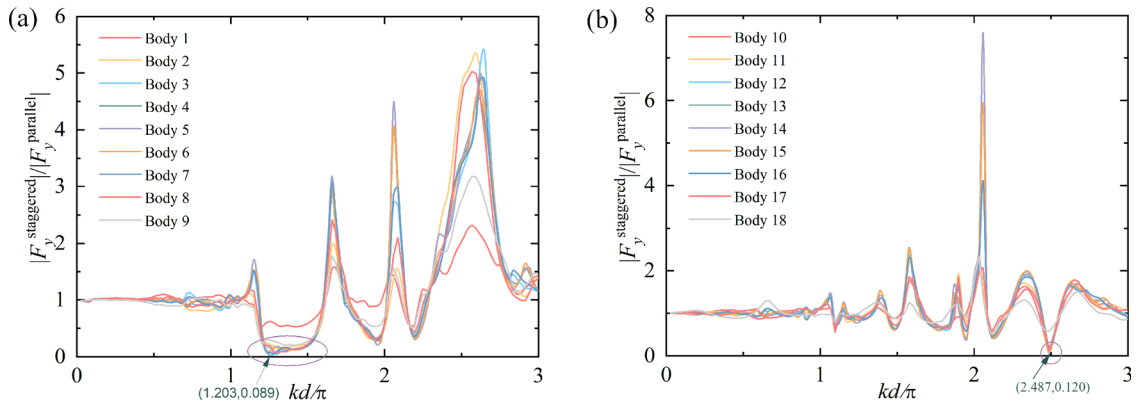

FIG. 22. Force enhancement ratios of the lateral force F_y acting on a 2×9 double staggered array over that on a 2×9 double parallel array in beam waves ($\beta = 90°$, $h = 50$ m, $s = 2D$): (a) the rear row and (b) the front row.

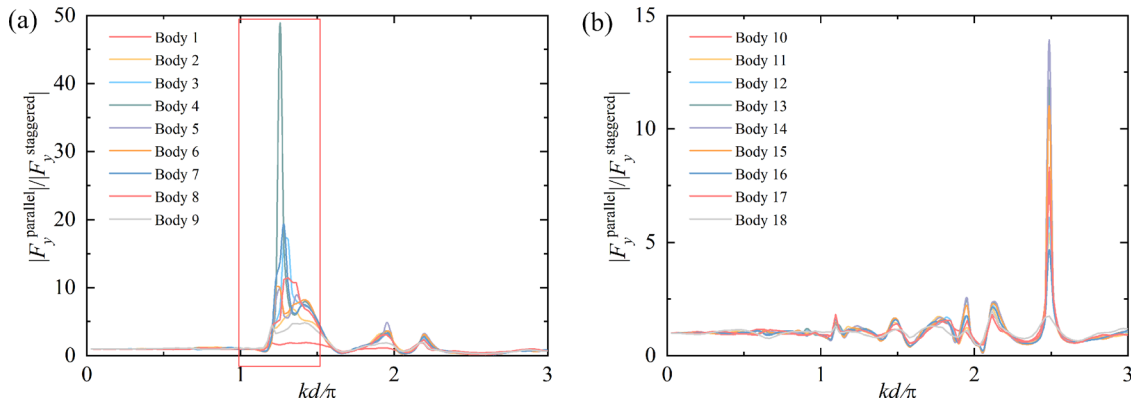

FIG. 23. Inverse force enhancement ratios of the lateral force F_y acting on a 2×9 double parallel array over that on a 2×9 double staggered array in beam waves ($\beta = 90°$, $h = 50$ m, $s = 2D$): (a) the rear row and (b) the front row.

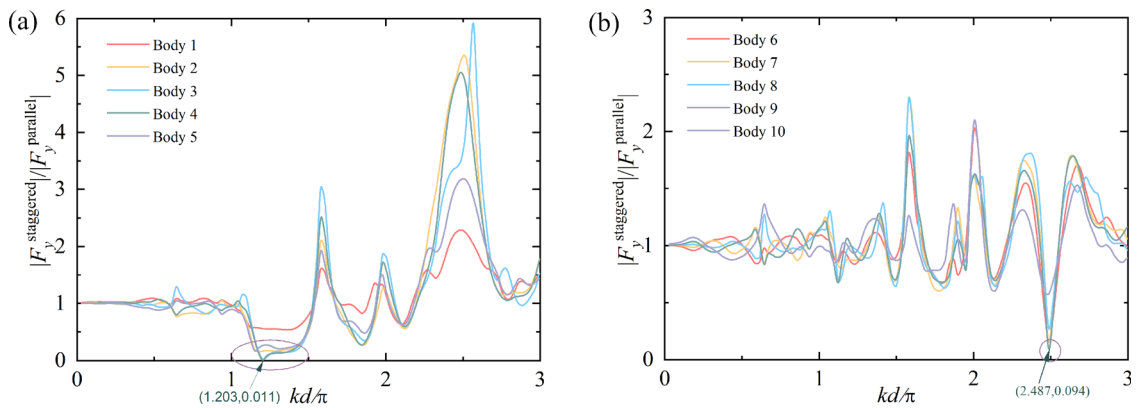

FIG. 24. Force enhancement ratios of the lateral force F_y acting on a 2×5 double staggered array over that on a 2×5 double parallel array in beam waves ($\beta = 90°$, $h = 50$ m, $s = 2D$): (a) the rear row and (b) the front row.

© Author(s) 2022

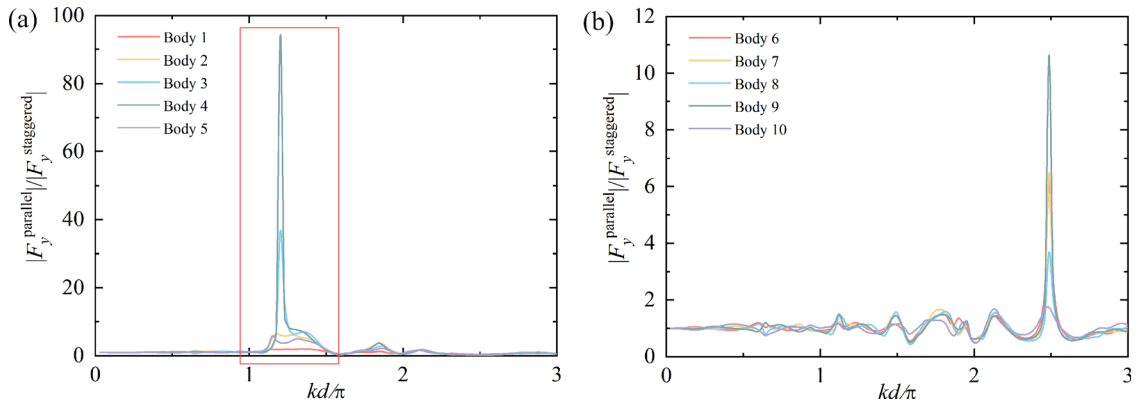

FIG. 25. Inverse force enhancement ratios of the lateral force F_y acting on a 2×5 double parallel array over that on a 2×5 double staggered array in beam waves ($\beta = 90°, h = 50\,\text{m}, s = 2D$): (a) the rear row and (b) the front row.

(1) In a uniform line array, trapped waves exist at critical wave numbers slightly less than a cutoff value $kd = n\pi/2\,(n \in \mathbb{N})$ in head waves. In beam waves, the longitudinal force F_x acting on each device is no more zero, except the one in the middle of the line array. The peak load on the middle device increases with the number of devices in head waves.

(2) In a double parallel array, there is no particular load enhancement as compared to the uniform line array in head waves, whereas in beam waves, significant load enhancement is found in the longitudinal and vertical forces. The longitudinal force on the middle device of either the front or the rear row is zero.

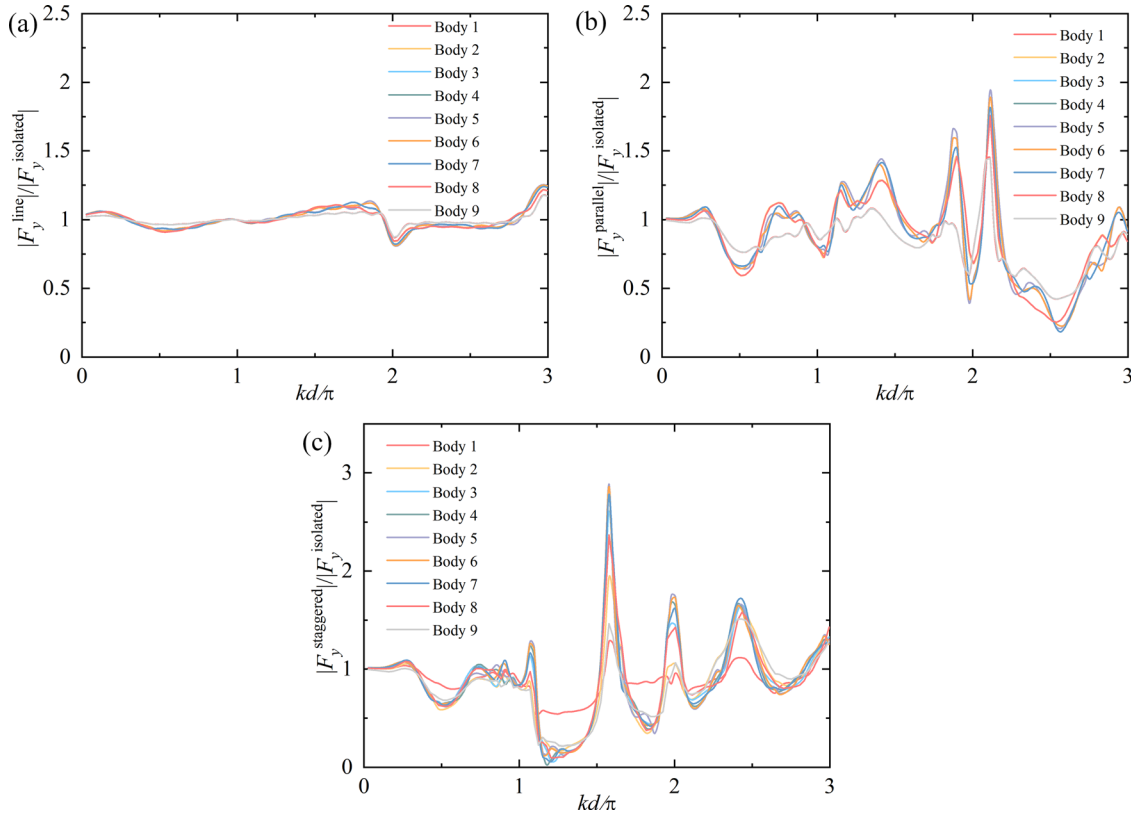

FIG. 26. Lateral force ratios of (a) a 1×9 uniform line array, (b) a 2×9 double parallel array, and (c) a 2×7 double staggered array over that of a single isolated device in beam waves ($\beta = 90°, h = 50\,\text{m}, s = 2D$).

© Author(s) 2022

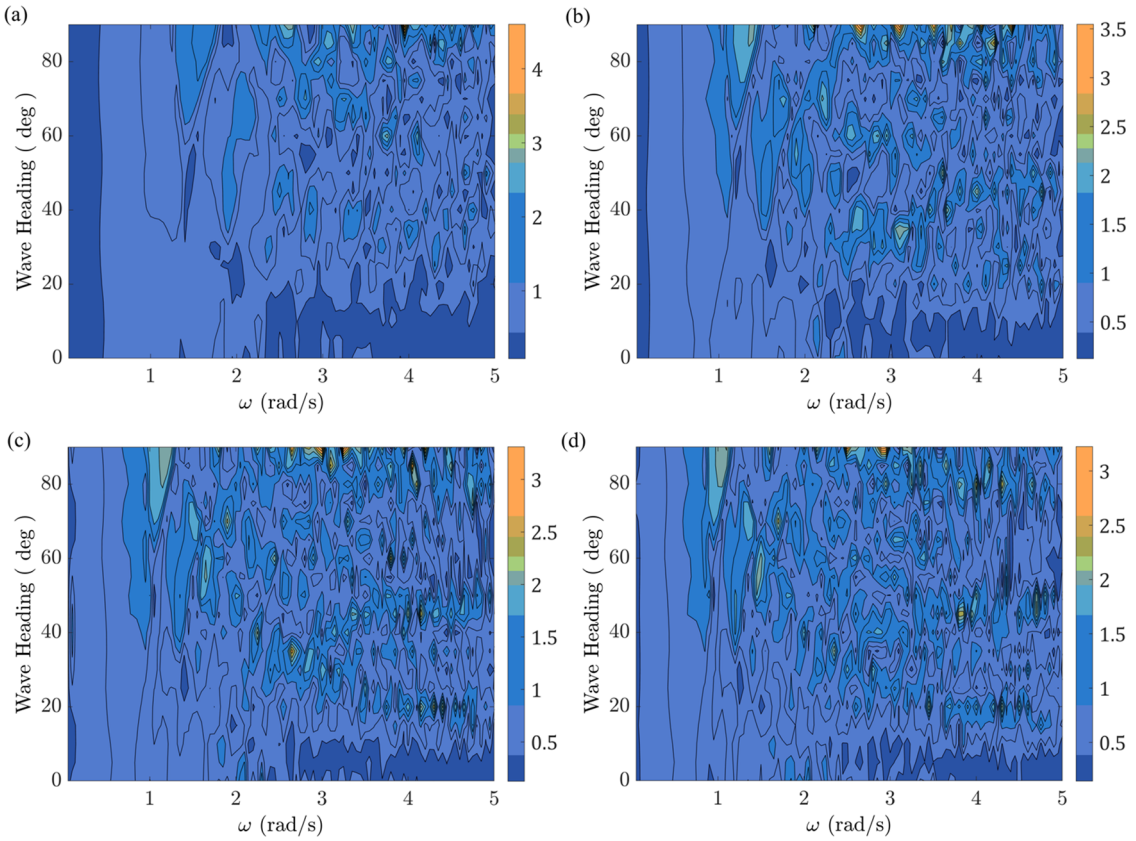

FIG. 27. q-factor variation of a 2×7 double staggered array of CorPower-like point absorbers against the angular frequency ω, the wave heading β, and the device spacing s ($h = 100$ m): (a) $s = 2D$, (b) $s = 3D$, (c) $s = 4D$, and (d) $s = 5D$.

(3) In a double staggered array, the lateral force in beam waves diminishes in between a narrow frequency bandwidth $kd/\pi \in [1.0, 1.5]$ and around $kd/\pi = 2.5$. Moreover, in long waves regimes, e.g., $kd/\pi < 1.0$, the staggered arrangement has little effect as compared to a double parallel array.
(4) The general principle of wave force variations is found as follows. In head waves, by extending a uniform line array to a double array, the longitudinal force magnitude remains at the same level, whereas a series of secondary peaks appear. In beam waves, with the increase in the array layout complexity, the lateral force in parallel to the wave propagation direction has a broader range of magnitude over the frequency band.
(5) The q-factor variations show that there are optimized regions in wave energy absorption against wave conditions. By arranging the array layout in a more randomized way, the optimal condition for maximized power output is hard to reach; however, the maximum power output increases to a higher level. Furthermore, the density of spot regions increases with the device spacing, and the areas of these regions vary with the frequency.

The above findings summarized in (1) and (2) are in line with those documented in Maniar and Newman (1997) that were concluded for a uniform line array of a regular geometry, i.e., bottom-mounted vertical circular cylinders, which can be viewed as the counterpart of the latter for an array of a non-regular geometry. The new findings regarding the uniform line array and the double parallel and staggered arrays are expected to benefit the design of wave energy arrays in practical applications.

ACKNOWLEDGMENTS

Y.L. acknowledges support from Grant-in-Aid for Early-Career Scientists (JSPS) [Grant Nos. JP18K13939 and JP22K14430]. S.Z. acknowledges support from Open Research Fund Program of State Key Laboratory of Hydroscience and Engineering (Tsinghua University) [Grant No. sklhse-2021-E-02]. The body surface mesh of the CorPower-like device provided by Iñaki Zabala of SENER Ingeniería y Sistemas, S.A., Spain, is greatly appreciated.

AUTHOR DECLARATIONS

Conflict of Interest

The authors have no conflicts to disclose.

Author Contributions

Yingyi Liu: Conceptualization (equal); Formal analysis (equal); Funding acquisition (equal); Investigation (equal); Methodology (equal); Project administration (equal); Validation (equal);

© Author(s) 2022

Visualization (equal); Writing – original draft (equal); Writing – review & editing (equal). **Siming Zheng:** Formal analysis (equal); Funding acquisition (equal); Investigation (equal); Methodology (equal); Project administration (equal); Validation (equal); Writing – review & editing (equal). **Hui Liang:** Formal analysis (equal); Investigation (equal); Methodology (equal); Writing – review & editing (equal). **Pei-wen Cong:** Formal analysis (equal); Investigation (equal); Methodology (equal); Writing – review & editing (equal).

DATA AVAILABILITY

The data that support the findings of this study are available from the corresponding or the first author upon reasonable request.

NOMENCLATURE

A	Ambient incident wave amplitude
a_j^I	Incident wave expansion coefficient to body j due to ambient incident wave
$a_j^{R,i,p}$	Incident wave expansion coefficient to body j due to unitary motion of body i in pth DoF
A_i^S	Scattered wave expansion coefficient of body i
d	Half device spacing
D	Device characteristic diameter
D_j	Diffraction transfer matrix of body j
DoF	Degree of freedom
$F_{j,p}^E$	Excitation force on body j in pth DoF
$F_{j,t}^{R,i,p}$	Radiation force on body j in tth DoF due to unitary motion of body i in pth DoF
$G_{j,p}^E$	Force transfer matrix of body j in pth DoF
h	Water depth
k	Wave number
R_i^p	Radiation characteristics of body j due to unitary motion in pth DoF
s	Full device spacing
β	Wave incident angle
η_j^E	Total wave elevation incidenting to body j due to ambient incident wave
$\eta_j^{R,i,p}$	Total wave elevation incidenting to body j due to unitary motion of body i in pth DoF
ϕ_j^A	Ambient incident wave potential to body j
ϕ_j^I	Total wave potential incidenting to body j
ϕ_i^S	Scattered wave potential from body i
ψ_j^I	Incident partial wave component to body j
ψ_j^S	Scattered partial wave component from body j
ω	Wave angular frequency

REFERENCES

Abramowitz, M., and Stegun, I. A., *Handbook of Mathematical Functions With Formulas, Graphs, and Mathematical Tables* (U.S. Government Printing Office, 1964), Vol. 55.

Babarit, A., "On the park effect in arrays of oscillating wave energy converters," Renewable Energy **58**, 68–78 (2013).

Bai, W., Feng, X., Eatock Taylor, R., and Ang, K., "Fully nonlinear analysis of near-trapping phenomenon around an array of cylinders," Appl. Ocean Res. **44**, 71–81 (2014).

Barbariol, F., Benetazzo, A., Carniel, S., and Sclavo, M., "Improving the assessment of wave energy resources by means of coupled wave-ocean numerical modeling," Renewable Energy **60**, 462–471 (2013).

Cheng, Y., Li, G., Ji, C., and Zhai, G., "Numerical investigation of solitary wave slamming on an oscillating wave surge converter," Phys. Fluids **31**, 037102 (2019).

Child, B., and Venugopal, V., "Optimal configurations of wave energy device arrays," Ocean Eng. **37**, 1402–1417 (2010).

Evans, D., "Some theoretical aspects of three-dimensional wave-energy absorbers," in *Proceedings of the 1st Symposium on Wave Energy Utilization Gothenburg, Sweden* (Chalmers University of Technology, 1979), pp. 78–112.

Evans, D., and Porter, R., "Near-trapping of waves by circular arrays of vertical cylinders," Appl. Ocean Res. **19**, 83–99 (1997).

Evans, D., and Porter, R., "Trapping and near-trapping by arrays of cylinders in waves," J. Eng. Math. **35**, 149–179 (1999).

Faedo, N., Scarciotti, G., Astolfi, A., and Ringwood, J. V., "Energy-maximising moment-based constrained optimal control of ocean wave energy farms," IET Renewable Power Gen. **15**, 3395–3408 (2021).

Falnes, J., "Radiation impedance matrix and optimum power absorption for interacting oscillators in surface waves," Appl. Ocean Res. **2**, 75–80 (1980).

Falnes, J., and Kurniawan, A., *Ocean Waves and Oscillating Systems: Linear Interactions Including Wave-Energy Extraction* (Cambridge University Press, 2020), Vol. 8.

Fitzgerald, C., and Thomas, G., "A preliminary study on the optimal formation of an array of wave power devices," in Proceedings of the 7th European Wave and Tidal Energy Conference, Porto, Portugal (2007), pp. 11–14.

Flavià, F. F., and Meylan, M. H., "An extension of general identities for 3D water-wave diffraction with application to the Diffraction Transfer Matrix," Appl. Ocean Res. **84**, 279–290 (2019).

Flavià, F. F., McNatt, C., Rongère, F., Babarit, A., and Clément, A. H., "A numerical tool for the frequency domain simulation of large arrays of identical floating bodies in waves," Ocean Eng. **148**, 299–311 (2018).

Gao, J., Ma, X., Dong, G., Chen, H., Liu, Q., and Zang, J., "Investigation on the effects of Bragg reflection on harbor oscillations," Coastal Eng. **170**, 103977 (2021).

Garnaud, X., and Mei, C. C., "Wave-power extraction by a compact array of buoys," J. Fluid Mech. **635**, 389–413 (2009).

Gomes, R. P., Gato, L. M., Henriques, J. C., Portillo, J. C., Howey, B. D., Collins, K. M., Hann, M. R., and Greaves, D. M., "Compact floating wave energy converters arrays: Mooring loads and survivability through scale physical modelling," Appl. Energy **280**, 115982 (2020).

Göteman, M., "Wave energy parks with point-absorbers of different dimensions," J. Fluids Struct. **74**, 142–157 (2017).

Guo, B., Patton, R., Jin, S., Gilbert, J., and Parsons, D., "Nonlinear modeling and verification of a heaving point absorber for wave energy conversion," IEEE Trans. Sustainable Energy **9**, 453–461 (2017).

Iglesias, G., and Carballo, R., "Offshore and inshore wave energy assessment: Asturias (N Spain)," Energy **35**, 1964–1972 (2010).

Isaacs, J. D., and Schmitt, W. R., "Ocean energy: Forms and prospects," Science **207**, 265–273 (1980).

Kagemoto, H., and Yue, D. K. P., "Interactions among multiple three-dimensional bodies in water waves: An exact algebraic method," J. Fluid Mech. **166**, 189–209 (1986).

Konispoliatis, D., and Mavrakos, S., "Hydrodynamic analysis of an array of interacting free-floating oscillating water column (OWC) devices," Ocean Eng. **111**, 179–197 (2016).

Li, Y., and Mei, C. C., "Bragg scattering by a line array of small cylinders in a waveguide. Part 1. Linear aspects," J. Fluid Mech. **583**, 161–187 (2007).

Linton, C., and Evans, D., "The interaction of waves with arrays of vertical circular cylinders," J. Fluid Mech. **215**, 549–569 (1990).

Liu, Y., "HAMS: A frequency-domain preprocessor for wave-structure interactions—Theory, development, and application," J. Mar. Sci. Eng. **7**, 81 (2019).

Liu, Y., Liang, H., Kashiwagi, M., and Cong, P., "Alternative approaches of evaluating diffraction transfer matrix and radiation characteristics using the hybrid source-dipole formulation," Appl. Ocean Res. **114**, 102769 (2021).

© Author(s) 2022

Malenica, S., Eatock Taylor, R., and Huang, J., "Second-order water wave diffraction by an array of vertical cylinders," J. Fluid Mech. **390**, 349–373 (1999).
Maniar, H., and Newman, J., "Wave diffraction by a long array of cylinders," J. Fluid Mech. **339**, 309–330 (1997).
McIver, P., "Wave interaction with arrays of structures," Appl. Ocean Res. **24**, 121–126 (2002).
McNatt, J. C., Venugopal, V., and Forehand, D., "A novel method for deriving the diffraction transfer matrix and its application to multi-body interactions in water waves," Ocean Eng. **94**, 173–185 (2015).
Meylan, M. H., and Eatock Taylor, R., "Time-dependent water-wave scattering by arrays of cylinders and the approximation of near trapping," J. Fluid Mech. **631**, 103–125 (2009).
Ning, D., Zhang, S., Chen, L., Liu, H.-W., and Teng, B., "Nonlinear Bragg scattering of surface waves over a two-dimensional periodic structure," J. Fluid Mech. **946**, A25 (2022).
Ogden, D., Ruehl, K., Yu, Y.-H., Keester, A., Forbush, D., Leon, J., and Tom, N., "Review of WEC-Sim development and applications," in Proceedings of the 14th European Wave and Tidal Energy Conference (EWTEC 2021), Plymouth, UK (2021), pp. 5–9.
Ohl, C., Eatock Taylor, R., Taylor, P., and Borthwick, A., "Water wave diffraction by a cylinder array. Part 1. Regular waves," J. Fluid Mech. **442**, 1–32 (2001).
Paduano, B., Giorgi, G., Gomes, R. P., Pasta, E., Henriques, J. C., Gato, L. M., and Mattiazzo, G., "Experimental validation and comparison of numerical models for the mooring system of a floating wave energy converter," J. Mar. Sci. Eng. **8**, 565 (2020).
Parrinello, L., Dafnakis, P., Pasta, E., Bracco, G., Naseradinmousavi, P., Mattiazzo, G., and Bhalla, A. P. S., "An adaptive and energy-maximizing control optimization of wave energy converters using an extremum-seeking approach," Phys. Fluids **32**, 113307 (2020).
Peng, J., Tao, A., Liu, Y., Zheng, J., Zhang, J., and Wang, R., "A laboratory study of class III Bragg resonance of gravity surface waves by periodic beds," Phys. Fluids **31**, 067110 (2019).
Pennock, S., Vanegas-Cantarero, M. M., Bloise-Thomaz, T., Jeffrey, H., and Dickson, M. J., "Life cycle assessment of a point-absorber wave energy array," Renewable Energy **190**, 1078–1088 (2022).
Siddorn, P., and Eatock Taylor, R., "Diffraction and independent radiation by an array of floating cylinders," Ocean Eng. **35**, 1289–1303 (2008).
Wang, C., and Wu, G., "Time domain analysis of second-order wave diffraction by an array of vertical cylinders," J. Fluids Struct. **23**, 605–631 (2007).
Wang, C., and Wu, G., "Interactions between fully nonlinear water waves and cylinder arrays in a wave tank," Ocean Eng. **37**, 400–417 (2010).
Wang, C., Zheng, S., and Zhang, Y., "A heaving system with two separated oscillating water column units for wave energy conversion," Phys. Fluids **34**, 047103 (2022).
Wolgamot, H., Taylor, P., and Eatock Taylor, R., "The interaction factor and directionality in wave energy arrays," Ocean Eng. **47**, 65–73 (2012).
Xu, S., Wang, S., and Soares, C. G., "Experimental investigation on hybrid mooring systems for wave energy converters," Renewable Energy **158**, 130–153 (2020).
Zeng, X., Yu, F., Shi, M., and Wang, Q., "Fluctuation of magnitude of wave loads for a long array of bottom-mounted cylinders," J. Fluid Mech. **868**, 244–285 (2019).
Zhao, X., Xue, R., Geng, J., and Göteman, M., "Analytical investigation on the hydrodynamic performance of a multi-pontoon breakwater-WEC system," Ocean Eng. **220**, 108394 (2021).
Zheng, S., Zhang, Y., and Iglesias, G., "Wave–structure interaction in hybrid wave farms," J. Fluids Struct. **83**, 386–412 (2018).
Zhong, Q., and Yeung, R. W., "Wave-body interactions among energy absorbers in a wave farm," Appl. Energy **233**, 1051–1064 (2019).

© Author(s) 2022